

FENE DUMBBELL MODEL AND ITS SEVERAL LINEAR AND NONLINEAR CLOSURE APPROXIMATIONS*

QIANG DU[†], CHUN LIU[†], AND PENG YU[†]

Abstract. We present some analytical and numerical studies on the finite extendible nonlinear elasticity (FENE) model of polymeric fluids and its several moment-closure approximations. The well-posedness of the FENE model is established under the influence of a steady flow field. We further infer existence of long-time and steady-state solutions for purely symmetric or antisymmetric velocity gradients. The stability of the steady-state solution for a general velocity gradient is illuminated by the analysis of the FENE-P closure approximation. We also propose a new linear closure approximation utilizing higher moments, which is shown to generate more accurate approximations than other existing closure models for moderate shear or extension rates. An instability phenomenon under a large strain is also investigated. This paper is a sequel to our earlier work [P. Yu, Q. Du, and C. Liu, *Multiscale Model. Simul.*, 3 (2005), pp. 895–917].

Key words. finite extendible nonlinear elasticity, non-Newtonian fluids, moment closure, finite extendible nonlinear elasticity-P, Fokker–Planck equation, stability analysis

AMS subject classifications. 76A05, 76M99, 65C30

DOI. 10.1137/040612038

1. Introduction. Non-Newtonian viscoelastic fluids comprise a large class of soft materials, such as polymeric solutions, liquid crystal solutions, electro(magneto)-rheological fluids, and fiber suspensions. The stress endured by a viscoelastic fluid element depends upon the history of the deformation experienced by that element, which is further attributable to the coupling between the flow-induced evolution of molecular configurations and macroscopic rheological response. This coupling calls naturally for the development of multiscale methods to analyze the flow of rheologically complex fluids. The multiscale models of viscoelastic fluids bridge directly the microscopic scale of kinetic theory and the macroscopic scale of continuum mechanics. Serving as the link between the two scales is the macroscopic stress carried by each material element which is determined by the distribution of the molecular configurations within that element. On the macroscopic level, the theory of continuum mechanics yields a force-balance law expressed, for instance, by the incompressible Navier–Stokes equation, except for the inclusion of an additional stress term accounting for the contribution from the coarse-grained microstructure. On the microscopic level, the kinetic theory gives a Fokker–Planck equation for the probability density function (PDF) $f(\vec{Q}, t)$, where \vec{Q} denotes the set of variables defining the coarse-grained microstructure [2, 5]. For example, dilute solutions of linear polymers can be described in some detail by a freely jointed bead-rod Kramers chain or, on a coarser level, by a freely jointed bead-spring chain. In this paper, we discuss an even coarser model of the single dumbbell, namely two beads connected by an elastic spring. In this case, the configuration variable \vec{Q} simply represents the vector connecting the two beads of the dumbbell.

*Received by the editors July 21, 2004; accepted for publication (in revised form) March 16, 2005; published electronically August 22, 2005. This research was supported in part by grants NSF DMS-0196522, NSF ITR-0205232, and NSF-DMS 0405850.

<http://www.siam.org/journals/mms/4-3/61203.html>

[†]Department of Mathematics, Pennsylvania State University, University Park, PA 16802 (qdu@math.psu.edu, liu@math.psu.edu, pyu@math.psu.edu).

Thus, the multiscale approach to modeling dilute solutions of flexible polymers (treated as dumbbells) involves solving the coupled PDEs consisting of the macroscopic momentum equation, the incompressible Navier–Stokes equation, and a Fokker–Planck equation describing the PDF $f = f(\vec{x}, \vec{Q}, t)$ of the dumbbell orientation \vec{Q} on the microscopic level. The coupled system [2] reads

$$(1.1) \quad \frac{\partial \vec{u}}{\partial t} + (\vec{u} \cdot \nabla) \vec{u} + \nabla p = \nabla \cdot \tau_p + \nu \Delta \vec{u},$$

$$(1.2) \quad \nabla \cdot \vec{u} = 0,$$

$$(1.3) \quad \frac{\partial f}{\partial t} + (\vec{u} \cdot \nabla) f + \nabla_{\vec{Q}} \cdot (\nabla \vec{u} \vec{Q} f) = \frac{2}{\zeta} \nabla_{\vec{Q}} \cdot (\nabla_{\vec{Q}} \Psi(\vec{Q}) f) + \frac{2kT}{\zeta} \Delta_{\vec{Q}} f.$$

In the Navier–Stokes equation (1.1), p is the hydrostatic pressure, ν is the fluid viscosity, and τ_p is a tensor representing the polymer contribution to stress,

$$(1.4) \quad \tau_p = \lambda \int (\nabla_{\vec{Q}} \Psi(\vec{Q}) \otimes \vec{Q}) f(\vec{x}, \vec{Q}, t) d\vec{Q},$$

where $\Psi(\vec{Q})$ is the elastic spring potential to be specified later, and λ is the polymer density constant. This induced elastic stress τ_p in (1.4) can be derived from the least action principle by looking at the variation of the following elastic part of the action function [5, 26]:

$$(1.5) \quad \lambda \delta \left(\int_0^T \int_{\Omega} \int_{R^3} K T f \ln f + \Psi f d\vec{Q} d\vec{x} dt \right) = \int_0^T \int_{\Omega} \int_{R^3} \tau_p : \nabla \delta \vec{x} d\vec{Q} d\vec{x} dt,$$

where δ represents the infinitesimal variation of the corresponding functions. In the Fokker–Planck equation (1.3), ζ is the friction coefficient of the dumbbell beads, T is the temperature, and k is the Boltzmann constant. The terms in (1.3) can be roughly explained as follows. The second and third terms on the left-hand side of (1.3) stem from the fact that the polymers are convected and stretched by the macroscopic flow, the first term on the right-hand side of (1.3) accounts for the inner force of the dumbbell due to the spring potential, and the last diffusion term on the right-hand side of (1.3) models the random collisions of the solvent particles with the polymers. This interpretation becomes clearer when we associate the Fokker–Planck equation (1.3) with the stochastic differential equation (SDE) [10]

$$(1.6) \quad d\vec{Q} + \vec{u} \cdot \nabla \vec{Q} dt = \left(\nabla \vec{u} \vec{Q} - \frac{2}{\zeta} \nabla_{\vec{Q}} \Psi \right) dt + \sqrt{\frac{4kT}{\zeta}} d\vec{W}_t,$$

where \vec{W}_t is the standard Brownian motion. This SDE defines Brownian dynamics of the connector vector \vec{Q} such as the fact that the probability distribution of dumbbell polymers evolves according to the Fokker–Planck equation (1.3). The Lagrangian version of (1.6) is given in [9], and for a discussion of various choices of the noise term W_t for variance reduction purposes, readers are referred to [13].

We note that for the kind of complex fluids we are considering here, the mechanical transport and deformation are only imposed by the macroscopic level. To illustrate this point, we explain the origin of the particular transport terms in (1.3), $\frac{\partial f}{\partial t} + (\vec{u} \cdot \nabla) f + \nabla_{\vec{Q}} \cdot (\nabla \vec{u} \vec{Q} f)$. For a given material point \vec{X} , we define the characteristic $\vec{x}(\vec{X}, t)$ such that

$$(1.7) \quad \vec{x}_t = \vec{u}(\vec{x}(\vec{X}, t), t), \quad \vec{x}(\vec{X}, 0) = \vec{X}.$$

Denoting F the deformation tensor $\frac{\partial \vec{x}}{\partial \vec{X}}$ and $\vec{q} = F^{-1}\vec{Q}$ the inverse stretching of the molecular orientation by the flow field, we can verify that

$$(1.8) \quad \frac{\partial f}{\partial t} + (\vec{u} \cdot \nabla)f + \nabla_{\vec{Q}} \cdot (\nabla \vec{u} \vec{Q} f) = \frac{D}{Dt} f(\vec{x}(\vec{X}, t), F\vec{q}, t).$$

Here we have used the identity [8, 21]

$$(1.9) \quad F_t + \vec{u} \cdot \nabla F = \nabla \vec{u} F,$$

which is a direct consequence of the chain rule.

The simplest spring potential is given by the Hookean law $\Psi(\vec{Q}) = HQ^2/2$, where $Q = |\vec{Q}|$ and H is the elasticity constant. In fact, exploiting this simple potential, one can derive a macroscopic differential constitutive equation for the polymeric stress τ_p from the Fokker–Planck equation, which leads to the so-called Oldroyd-B fluids. However, for a more practical finite extendible nonlinear elasticity (FENE) potential that takes into account a finite-extensibility constraint, $\Psi(\vec{Q}) = -(HQ_0^2/2) \log(1 - (Q/Q_0)^2)$, there does not exist an exact macroscopic constitutive equation for τ_p , and thus the FENE model represents a truly multiscale model. Here Q_0 is the maximum dumbbell extension. The FENE spring force law reads

$$(1.10) \quad \nabla_{\vec{Q}} \Psi = \frac{H\vec{Q}}{1 - (Q/Q_0)^2}.$$

The goal of this paper is to study several analytical and numerical issues related to the FENE model.

For one-dimensional shear flows, the well-posedness of the system coupling the Navier–Stokes equations and the SDE (1.6) with the FENE potential has been established by Jourdain, Lelievre, and Le Bris [14] using the specific simple structure of shear flow. To extend such analysis to higher dimension, a crucial step has been done by E, Li, and Zhang [6] to analyze the local well-posedness of the coupled system. On the other hand, there is much less analytical work on the Fokker–Planck equation itself. Lin, Liu, and Zhang [19] recently proved well-posedness of the flow system coupled with the Fokker–Planck equation for Hookean potential (the existence of global classical solutions when the initial datum are near the equilibrium configurations). Li, Zhang, and Zhang [20] have established local existence of the same system when the force law satisfies polynomial growth condition.

It is important to note that the added complexity with the FENE potential affects mostly the analysis of the underlying Fokker–Planck equation, such as the issue of boundary conditions as well as the singularity of coefficients near the boundary of the configuration domain. Hence, in this paper, we present the well-posedness of the Fokker–Planck equation alone, with the fluid velocity being steady and homogeneous. In other words, we suppress the convective term $\vec{u} \cdot \nabla f$ in (1.3), and the velocity gradient ∇u is treated as a constant matrix. We note that, independently from our work here, a preliminary analysis of the coupled system with the FENE potential was made recently [27]. The approach used there, however, is different from what we employ here, and the well-posedness results established in [27] were also under more restrictive assumptions on the maximum extension rate than what are required here. The major difficulty is to select the appropriate functional space such that the degeneracy of the FENE potential at the boundary $\vec{Q} = Q_0$ can be treated naturally. Upon choosing the suitable space, we show finite-time existence of the solution to

the Fokker–Planck equation for general velocity gradients and show global-in-time existence of the solution in the case where the velocity gradients are purely symmetric or antisymmetric. We mention that such a “decoupled” study for the SDE (1.6) has been carried out by Jourdain and Lelievre [11] with a detailed discussion on the dependence of the existence and uniqueness of the solution on the finite-extensibility parameter. The approach there is, of course, very different.

Simulating the coupled micro-macro system numerically is a demanding task, in that at each spatial point \vec{x} , the configuration space of \vec{Q} needs to be resolved or at least sampled. Recently, Lozinski and Chauviere [22] have introduced a fast solver to tackle the Fokker–Planck equation directly with a novel time splitting scheme. However, a more widely used method to solve the coupled system is the so-called CONNFESSIT approach [15, 23] that simulates the SDE corresponding to the Fokker–Planck equation to achieve a Monte Carlo sampling of the configuration space. The latter approach has the advantage that the complexity increases only linearly with the number of beads of the multibead polymer chains. We will briefly review the Monte Carlo simulation of the FENE model and present a finite-difference scheme used later in this paper which has several attractive features, such as simplicity and positivity preserving. Our focus regarding numerical simulation of the FENE model, however, is on the so-called moment-closure approach.

To illustrate the idea of moment-closure approximations, we multiply the Fokker–Planck equation in two dimensions by $\vec{Q} \otimes \vec{Q}$ and perform integration by parts on the probability space $|\vec{Q}| < Q_0$. Denoting by A the conformation tensor $\langle \vec{Q} \otimes \vec{Q} \rangle$, where the brackets represent the ensemble average over the space $|\vec{Q}| < Q_0$, i.e., $\langle \vec{Q} \otimes \vec{Q} \rangle \equiv \int_{|\vec{Q}| < Q_0} \vec{Q} \otimes \vec{Q} f(\vec{x}, \vec{Q}, t) d\vec{Q}$, we get

$$(1.11) \quad \frac{\partial A}{\partial t} + (\vec{u} \cdot \nabla)A - (\nabla u)A - A(\nabla u)^T = -\frac{4}{\zeta} \int \frac{H\vec{Q} \otimes \vec{Q}}{1 - Q^2/Q_0^2} f(x, \vec{Q}, t) d\vec{Q} + \frac{4kT}{\zeta}.$$

If we select the conformation tensor as the only *state variable*, to close the equation, it is necessary to find an approximate relation to represent the ensemble average term $\langle \frac{H\vec{Q} \otimes \vec{Q}}{1 - Q^2/Q_0^2} \rangle$ on the right-hand side in terms of A . If done properly, this closure approach reduces the need to resolve the probability space and thus results in dramatic savings computationally. Certainly, the challenge is to find a *good* closure approximation, which is often not an easy task. Since no closure model is expected to give quantitative agreement with the original FENE model for all ranges of velocity gradients, a good model would be one that agrees quantitatively with the FENE model for certain regimes of the physical parameters and at least reproduces the qualitative behavior of the FENE model for other choices of the physical parameters.

A particularly simple closure approximation is the FENE-P closure based on an ad hoc preaveraging assumption,

$$(1.12) \quad \left\langle \frac{H\vec{Q} \otimes \vec{Q}}{1 - Q^2/Q_0^2} \right\rangle \approx \frac{H\langle \vec{Q} \otimes \vec{Q} \rangle}{\langle 1 - Q^2/Q_0^2 \rangle} = \frac{HA}{1 - \text{tr} A/Q_0^2}.$$

The FENE-P model has been used widely in qualitative studies of FENE fluids (see, for example, [28] and the references therein). But it is known that quantitative prediction of polymeric stress using FENE-P can deviate significantly from the original FENE model, even for considering only the steady state [28]. Furthermore, the time-dependent behavior of the FENE-P model is qualitatively different from that of the

FENE model, in that the hysteretic behavior of FENE fluids is lost [16]. As opposed to the ad hoc closure, a more systematic strategy to derive closure approximation is based on making an ansatz on the class of functions that the PDF solution to the Fokker–Planck equation can take. The merit of this approach lies in the fact that any closure relation derived this way is backed up by some underlying PDF and thus is kept from producing totally unrealistic predictions. Moreover, the resulting system may still keep certain energy law. On the other hand, the success of such methods clearly depends on how well the assumed class can capture the actual solution to the Fokker–Planck equation. An application of this strategy to the FENE model is given by Lielens et al. [16] and Lielens, Keunings, and Legat [17] and is named the FENE-L closure. They assume that the PDF $f = f(\vec{Q})$ takes a factored form,

$$(1.13) \quad f(\vec{Q}) = \psi^l(Q)\psi^o(\vec{Q}/Q),$$

where $\psi^l(Q)$ and $\psi^o(\vec{Q}/Q)$ are the distribution of the dumbbell’s length and unit orientation vector, respectively. The length distribution is further assumed to take an L-shaped form assembled from the Dirac- δ and Heaviside functions, i.e.,

$$(1.14) \quad Q\psi^l(Q) = \frac{1-\beta}{\alpha}(1-H_\alpha(Q)) + \beta\delta_\alpha(Q),$$

where $(\alpha, \beta) \in [0, \sqrt{b}] \times [0, 1]$ are parameters to be determined from the second-order moments $A = \langle Q \otimes Q \rangle$ and a fourth-order moment $\langle Q^4 \rangle$. Here $b = HQ_0^2/kT$. Leaving the orientation distribution $\psi^o(\vec{Q}/Q)$ unspecified, one may express the ensemble average $\langle \frac{H\vec{Q} \otimes \vec{Q}}{1-Q^2/Q_0^2} \rangle$ as an explicit function of α and β , which are in turn expressed in terms of the selected moments. One thus arrives at an explicit system of equations describing the evolution of state variables A and $\langle Q^4 \rangle$. The use of singular distributions in the ansatz (1.14) is motivated by the observation in numerical simulations that the true solution to the FENE Fokker–Planck equation can become rather singular for large shear or extension rates. Therefore, the FENE-L model has the advantage of being able to capture PDFs far away from the equilibrium. Its capability to qualitatively recover the hysteretic behavior of the original FENE fluids has also been shown.

We have recently proposed a closure model [25] based on restricting the PDFs to a class viewed as a perturbation to the equilibrium distribution. Taking two dimensions as an example, the ansatz reads

$$(1.15) \quad f(\vec{Q}) = \frac{1}{J_c} \left[1 - \left(\frac{Q}{Q_0} \right)^2 \right]^{c/2} (1 + \beta Q_1 Q_2 + \gamma(Q_1^2 - Q_2^2)),$$

where $\vec{Q} = (Q_1, Q_2)$, and J_c is scaling constant such that $\int f(\vec{Q})d\vec{Q} = 1$. When the three parameters c , β , and γ take the values HQ_0^2/kT , 0, and 0, respectively, the ansatz reduces to the equilibrium distribution of the FENE model. It is this explicit incorporation of the equilibrium distribution that distinguishes this model from FENE-P and FENE-L. It is shown in [25] that excellent agreement is obtained with the FENE model for shear flow with small shear rates and for coupled simulation of two-dimensional driven-cavity flow. However, it is also observed that the approximation deteriorates as the distortion on the PDF by the flow becomes stronger. In order to improve the closure approximation at larger shear or extension rates, we propose in this paper an improved closure that allows systematic inclusion of higher-order moments. The higher moment-closure relation is derived based on a similar framework,

except that the dependence of the ensemble average term needing closure on moments is linear, while the relation is nonlinear in all the previous closure models. We will show that, for moderate shear and extension rates, the closure based on higher-order moments produces much better stress predictions than the existing closure models, and increasing the order of moments involved results in better quantitative agreement with the FENE model. However, the deficiency of the model is that the moment equations become unstable for large shear or extension rates. This can be attributed to the linear nature of the closure relation which fails to control the growing eigenvalue of the linear system as the shear or extension rate increases. Stability analysis of this model as well as the FENE-P model will be carried out. In summary, the new higher moment-closure model outperforms the FENE-P or FENE-L models for moderate shear or extension flow rates but fails for large flow rates, whereas the FENE-P or FENE-L models do not.

The rest of the paper is organized as follows. We first address the well-posedness of the Fokker–Planck equation with a constant velocity gradient in section 2. Then we discuss its numerical simulations in section 3. The stability analysis of the FENE-P model is presented in section 4, and a higher-order moment-closure approximation is presented in section 5. A conclusion is given in section 6. We note that the results presented in the various sections of this paper are centered around the FENE model and its difficulties in both analysis and computing, in particular the singularity of the FENE force law. Our attempts in proving existence, building higher-order closure models, analyzing stability or instability, and developing suitable numerical schemes all illustrate the influence of this difficulty and also shed light on how it may be dealt with.

2. Well-posedness of the Fokker–Planck equation. As mentioned before, we constrain ourselves with studying the Fokker–Planck equation alone, decoupled from the flow calculation. Upon applying a standard scaling [9], the Fokker–Planck equation (1.3) reduces to

$$(2.1) \quad \frac{\partial f}{\partial t}(\vec{Q}, t) + \nabla_{\vec{Q}} \cdot (\kappa \vec{Q} f) = \frac{1}{2}(\nabla_{\vec{Q}} \cdot (\nabla_{\vec{Q}} \Psi f) + \Delta_{\vec{Q}} f),$$

where the FENE potential is such that

$$(2.2) \quad \nabla_{\vec{Q}} \Psi = \frac{\vec{Q}}{1 - Q^2/b}.$$

Here $\kappa = \nabla u$ is the steady homogeneous velocity gradient. We assume incompressible flow field u ; hence κ is traceless. The Fokker–Planck equation is defined on the open ball $\Omega = \{\vec{Q} \in \mathbb{R}^n : Q^2 < b\}$, where $n = 2, 3$. Typical values of b are 20, as in [22], and 50, as in [9, 16].

We first note that the operator $\mathcal{A}f = \frac{1}{2}(\nabla_{\vec{Q}} \cdot (\nabla_{\vec{Q}} \Psi f) + \Delta_{\vec{Q}} f)$ on the right-hand side of the Fokker–Planck equation has some nice mathematical properties. More specifically, \mathcal{A} as an operator on the functional space $\{f : e^{\Psi(\vec{Q})/2} f \in L^2(\Omega)\}$ is self-adjoint and coercive on the orthogonal of its null space [4]. However, for the solution f to represent a PDF, (2.1) needs to be conservative, and a major difficulty is to assign a meaning to the formal natural boundary condition

$$(2.3) \quad \left(\frac{1}{2}(\nabla_{\vec{Q}} \Psi f + \nabla_{\vec{Q}} f) - \kappa \vec{Q} f \right) \cdot \vec{n} |_{\partial\Omega} = 0,$$

for $\nabla_{\vec{Q}}\Psi$ is singular at the boundary of $\partial\Omega$. To circumvent this problem, we introduce the following transformation:

$$(2.4) \quad f(\vec{Q}, t) = e^{-\Psi(\vec{Q})/2} g(\vec{Q}, t).$$

It is easy to check that $g(\vec{Q}, t)$ satisfies

$$(2.5) \quad \frac{\partial g}{\partial t} + \nabla_{\vec{Q}} \cdot (\kappa \vec{Q} g) - \frac{\nabla_{\vec{Q}} \Psi \cdot \kappa \vec{Q}}{2} g = \frac{1}{4} \left(\Delta_{\vec{Q}} \Psi - \frac{1}{2} |\nabla_{\vec{Q}} \Psi|^2 \right) g + \frac{1}{2} \Delta_{\vec{Q}} g.$$

Terms involving $\nabla_{\vec{Q}} \Psi \cdot \nabla_{\vec{Q}} g$ have been cancelled due to our choice of the factor 2 in (2.4), and this is inherently linked to the properties of the self-adjoint operator \mathcal{A} mentioned above. The cancellation of $\nabla_{\vec{Q}} \Psi \cdot \nabla_{\vec{Q}} g$ also makes it easier to define the proper space in which the existence of solution to (2.5) is proved. We note that in the analysis of the fully coupled system given by Zhang [27], approximations (regularizations) were made on the singular coefficients.

In terms of the new function g , the original no-flux boundary condition (2.3) becomes

$$(2.6) \quad \left(\frac{1}{4} \nabla_{\vec{Q}} \Psi e^{-\Psi/2} g + e^{-\Psi/2} \left(\frac{1}{2} \nabla_{\vec{Q}} g - g \right) \right) \cdot \vec{n} \Big|_{\partial\Omega} = 0.$$

Since $e^{-\Psi/2} = (1 - Q^2/b)^{b/4}$, the singularity caused by $\nabla_{\vec{Q}} \Psi$ in (2.3) has been removed, as long as $b > 4$. Hereafter, we make the assumption that $b > 4$, and this assumption is reasonable for practical purposes since, according to [23], b is roughly the number of monomer units represented by a bead; thus it generally exceeds 10. But we mention that this constraint on b is not optimal mathematically, for it is known that the solution to the SDE associated with (2.1) exists and has trajectorial uniqueness if and only if $b \geq 2$ [11].¹ Now our goal is to establish the finite-time existence of the solution g to (2.5), and through the transformation (2.4) we then obtain the solution to the Fokker–Planck equation (2.1) which automatically satisfies the natural boundary condition, given certain regularity properties on g near the domain boundary. Thus, ideally, we would not have to impose any extra boundary conditions on (2.5) for g . However, as we exploit the transformation (2.4) to suppress the boundary singularity, we pay a price of losing the probability structure of the original Fokker–Planck equation. In particular, to prevent boundary terms from arising when carrying out integration by parts in the following analysis, we need to impose an extra homogeneous Dirichlet boundary condition on g . This does not affect the quality of the result because we are establishing the existence of the solution under more restrictive conditions. But, philosophically, it is not completely satisfactory because the reformulation of the original problem as in (2.5) where we request $g \in H_0^1(\Omega)$ is only partially consistent with the Fokker–Planck equation (2.1).

Let $V = \{g : \int_{\Omega} |\frac{g}{1-Q^2/b}|^2 d\vec{Q} < \infty\}$, which is equipped with the norm $\|g\|_V = \int_{\Omega} |\frac{g}{1-Q^2/b}|^2 d\vec{Q}$.

It is easy to verify that V is weakly compact and the set of smooth functions with compact support on Ω is dense in V . We further consider the functional space

¹The well-posedness of the Fokker–Planck equation with the FENE law has been established in a recent paper [1] for $b > 2$ with a smoothed velocity using similar but more complicated techniques as here. But we were unaware of this work at the time of writing this paper.

$H_0^1(\Omega) \cap V$ with the norm $\|g\|_{H^1} + \|g\|_V$. Given any finite time T , we will seek a weak solution to (2.5) in $X = L^\infty([0, T]; L^2(\Omega)) \cap L^2([0, T]; H_0^1(\Omega) \cap V)$. We state the weak formulation of (2.5): $g \in X$ is a weak solution to (2.5) if and only if for all $h \in H_0^1(\Omega) \cap V$ we have, in the sense of distributions,

$$(2.7) \quad \begin{aligned} \frac{d}{dt}(g, h) &= \int_{\Omega} \frac{1}{4} \left(\Delta_{\vec{Q}} \Psi - \frac{1}{2} |\nabla_{\vec{Q}} \Psi|^2 \right) gh d\vec{Q} - \frac{1}{2} \int_{\Omega} \nabla_{\vec{Q}} g \cdot \nabla_{\vec{Q}} h d\vec{Q} \\ &+ \int_{\Omega} \left(\frac{1}{2} \nabla_{\vec{Q}} \Psi g - \nabla_{\vec{Q}} g \right) \cdot \kappa \vec{Q} h d\vec{Q} \quad \forall t \in [0, T], \end{aligned}$$

and g satisfies the initial condition

$$(2.8) \quad g(0, \vec{Q}) = g_0(\vec{Q}) \quad \forall \vec{Q} \in \Omega,$$

where (g, h) denotes the L^2 inner product $\int_{\Omega} gh d\vec{Q}$. The initial condition makes sense because any solution to (2.7) will automatically be continuous from $[0, T]$ to V (after a modification on a zero measure set) [24].

To study the well-posedness of (2.7), we use the Galerkin method. Given a sequence of linearly independent smooth functions with compact support on Ω , $h_1, h_2, \dots, h_m, \dots$, which is total in the separable space $H_0^1(\Omega) \cap V$, for each m , we define an approximate solution g_m of (2.7) as follows:

$$(2.9) \quad g_m = \sum_{i=1}^m c_{im}(t) h_i$$

and

$$(2.10) \quad \begin{aligned} \frac{d}{dt}(g_m, h_j) &= \int_{\Omega} \frac{1}{4} \left(\Delta_{\vec{Q}} \Psi - \frac{1}{2} |\nabla_{\vec{Q}} \Psi|^2 \right) g_m h_j d\vec{Q} - \frac{1}{2} \int_{\Omega} \nabla_{\vec{Q}} g_m \cdot \nabla_{\vec{Q}} h_j d\vec{Q} \\ &+ \int_{\Omega} \left(\frac{1}{2} \nabla_{\vec{Q}} \Psi g_m - \nabla_{\vec{Q}} g_m \right) \cdot \kappa \vec{Q} h_j d\vec{Q}, \quad j = 1, \dots, m, \end{aligned}$$

$$(2.11) \quad g_m(0) = g_{0m},$$

where g_{0m} is the orthogonal projection in $H_0^1(\Omega) \cap V$ of g_0 on the space spanned by h_1, h_2, \dots, h_m .

It is easy to see that g_m is well defined. Moreover, we have the following theorem.

THEOREM 2.1. *For any given finite time T and $b > 4$, there exists a solution to (2.7) satisfying the initial condition (2.8), which is the weak limit point of $\{g_m\}$.*

Proof. The system (2.10) constitutes a linear system of ODEs with constant coefficients for the scalar functions $c_{im}(t)$. Together with the initial condition, this linear system defines uniquely the c_{im} on the whole interval $[0, T]$. Obviously, the approximate solutions g_m thus obtained belong to the solution space X .

To pass to the limit, we obtain a priori estimates independent of m for the functions g_m . We multiply (2.10) by c_{jm} and sum over $j = 1, \dots, m$. We get

$$(2.12) \quad \begin{aligned} \frac{d}{dt} \|g_m\|_{L^2}^2 &= \int_{\Omega} \frac{1}{4} \left(\Delta_{\vec{Q}} \Psi - \frac{1}{2} |\nabla_{\vec{Q}} \Psi|^2 \right) g_m^2 d\vec{Q} - \frac{1}{2} \int_{\Omega} |\nabla_{\vec{Q}} g_m|^2 d\vec{Q} \\ &+ \int_{\Omega} \left(\frac{1}{2} \nabla_{\vec{Q}} \Psi g_m + \nabla_{\vec{Q}} g_m \right) \cdot \kappa \vec{Q} g_m d\vec{Q}. \end{aligned}$$

Here we have used the fact that $\int_{\Omega} \nabla_{\vec{Q}} g_m \cdot \kappa \vec{Q} g_m d\vec{Q} = 0$ because κ is traceless and g_m 's satisfy zero boundary conditions. Performing integration by parts on $\int_{\Omega} \Delta_{\vec{Q}} \Psi g_m^2 d\vec{Q}$, one may easily verify that the above can be rewritten as

$$(2.13) \quad \frac{d}{dt} \|g_m\|_{L^2}^2 = -\frac{1}{2} \int_{\Omega} \left| \frac{1}{2} \nabla_{\vec{Q}} \Psi g_m + \nabla_{\vec{Q}} g_m \right|^2 d\vec{Q} + \int_{\Omega} \left(\frac{1}{2} \nabla_{\vec{Q}} \Psi g_m + \nabla_{\vec{Q}} g_m \right) \cdot \kappa \vec{Q} g_m d\vec{Q}.$$

The right-hand side is majorized by $\frac{1}{2} \int |\kappa \vec{Q} g_m|^2 d\vec{Q} \leq \frac{1}{2} \tilde{\kappa}^2 b \int |g_m|^2 d\vec{Q}$, where $\tilde{\kappa}$ is twice (in two dimensions) or triple (in three dimensions) the largest element (in magnitude) of κ . Integrating from 0 to s , $0 < s < T$, we have

$$(2.14) \quad \|g_m(s)\|_{L^2}^2 \leq \|g_{0m}\|_{L^2}^2 e^{\tilde{\kappa}^2 b s / 2}.$$

Hence

$$(2.15) \quad \sup_{s \in [0, T]} \|g_m(s)\|_{L^2}^2 \leq \|g_{0m}\|_{L^2}^2 e^{\tilde{\kappa}^2 b T / 2} \leq \|g_0\|_{L^2}^2 e^{\tilde{\kappa}^2 b T / 2}.$$

Hence we have a uniform bound on g_m in $L^\infty([0, T]; L^2(\Omega))$.

On the other hand, if we majorize the right-hand side of (2.13) by

$$-\frac{1}{4} \int_{\Omega} \left| \frac{1}{2} \nabla_{\vec{Q}} \Psi g_m + \nabla_{\vec{Q}} g_m \right|^2 d\vec{Q} + \int |\kappa \vec{Q} g_m|^2 d\vec{Q}$$

and integrate from 0 to T , we get a uniform bound on $\int_0^T \int_{\Omega} \left| \frac{1}{2} \nabla_{\vec{Q}} \Psi g_m + \nabla_{\vec{Q}} g_m \right|^2 d\vec{Q} dt$ independent of m . However, what we need are uniform bounds on $\int_0^T \int_{\Omega} |\nabla_{\vec{Q}} \Psi g_m|^2 d\vec{Q} dt$ (or equivalently $\int_0^T \int_{\Omega} \left| \frac{g_m}{1 - Q^2/b} \right|^2 d\vec{Q} dt$) and on $\int_0^T \int_{\Omega} |\nabla_{\vec{Q}} g_m|^2 d\vec{Q} dt$ separately. To this end, we return to (2.12). The right-hand side of (2.12) can be reorganized into

$$(2.16) \quad \int_{\Omega} \left(\frac{1}{4} \Delta_{\vec{Q}} \Psi - \frac{1}{8} |\nabla_{\vec{Q}} \Psi|^2 + \frac{1}{2} \nabla_{\vec{Q}} \Psi \cdot \kappa \vec{Q} \right) g_m^2 d\vec{Q} - \frac{1}{2} \int_{\Omega} |\nabla_{\vec{Q}} g_m|^2 d\vec{Q},$$

where we have used again the fact that κ is traceless. Direct computation shows

$$(2.17) \quad \frac{1}{4} \Delta_{\vec{Q}} \Psi - \frac{1}{8} |\nabla_{\vec{Q}} \Psi|^2 + \frac{1}{2} \nabla_{\vec{Q}} \Psi \cdot \kappa \vec{Q} = \frac{1}{2} \frac{d/2(1 - Q^2/b) + (1/b - 1/4)Q^2 + (1 - Q^2/b)\vec{Q} \cdot \kappa \vec{Q}}{(1 - Q^2/b)^2},$$

where $d = 2, 3$ is the dimensionality. For $Q^2 = b$, since $b > 4$, we have

$$d/2(1 - Q^2/b) + (1/b - 1/4)Q^2 + (1 - Q^2/b)\vec{Q} \cdot \kappa \vec{Q} = 1 - b/4 < 0.$$

Thus, there exist $r > 0$ and $\epsilon > 0$, such that $d/2(1 - Q^2/b) + (1/b - 1/4)Q^2 + (1 - Q^2/b)\vec{Q} \cdot \kappa \vec{Q} < -\epsilon$ for $|Q| > r$. If we split the first integral in (2.16) into two integrals over the domain $|Q| < r$ and $|Q| > r$, respectively, and integrate (2.12) from 0 to T , we get

$$(2.18) \quad \epsilon \int_0^T \int_{r^2 < Q^2 < b} \left| \frac{g_m}{1 - Q^2/b} \right|^2 d\vec{Q} dt \leq C \int_0^T \|g_m(s)\|_{L^2}^2 ds - \int_0^T \|\nabla g_m(s)\|_{L^2}^2 ds - (\|g_m(T)\|_{L^2}^2 - \|g_m(0)\|_{L^2}^2),$$

where C is a constant independent of m . In conjunction with (2.15), this shows at the same time that both $\int_0^T \int_{\Omega} |\frac{g_m}{1-Q^2/b}|^2 d\vec{Q} dt$ and $\int_0^T \int_{\Omega} |\nabla_{\vec{Q}} g_m|^2 d\vec{Q} dt$ are uniformly bounded independent of m ; hence we have the uniform bound on g_m in $L^2([0, T], H_0^1(\Omega) \cap V)$.

Finally, using the fact that the spaces V and $H_0^1(\Omega) \cap V$ are weakly compact, we can subtract a subsequence of g_m that converges weakly in X to a weak solution of (2.7). Since the equation of g is linear, this procedure of passing to the limit is trivial. For details of similar arguments, one may see, for example, [24]. \square

REMARK 1. Equation (2.13) can be estimated in a different way from the above proof of the theorem, namely, using the Cauchy-Schwarz inequality and a weighted Poincaré inequality

$$(2.19) \quad \int_{\Omega} e^{-\Psi} f^2 d\vec{Q} \leq \frac{1}{c} \int_{\Omega} e^{-\Psi} |\nabla f|^2 d\vec{Q} + \alpha \left(\int_{\Omega} e^{-\Psi} f d\vec{Q} \right)^2$$

for any f such that $e^{-\Psi/2} f \in H_0^1(\Omega)$. Here $c > 0$ is a constant, Ψ may be any function such that $\nabla^2 \Psi \geq cI$, and $\alpha^{-1} = \int_{\Omega} e^{-\Psi} d\vec{Q} < \infty$. We now outline a proof of the weighted Sobolev imbedding inequality due to R. Varadhan which might be of use to those interested in the analytical study of Fokker-Planck equations. First, let us define the operator

$$(2.20) \quad L = e^{\Psi} \nabla (e^{-\Psi} \nabla) = \Delta - \nabla \Psi \nabla$$

over the domain $e^{-\Psi/2} f \in H_0^1(\Omega)$. We notice that L is the dual operator of the original Fokker-Planck operator. Now consider the equation

$$(2.21) \quad u_t = Lu, \quad u(\cdot, 0) = f(\cdot),$$

and define the quantity:

$$(2.22) \quad D(t) = \int_{\Omega} e^{-\Psi} |u|^2 d\vec{Q},$$

and

$$(2.23) \quad H(t) = \int_{\Omega} e^{-\Psi} |\nabla u|^2 d\vec{Q}.$$

We see that

$$(2.24) \quad \frac{d}{dt} D(t) = \int_{\Omega} e^{-\Psi} u u_t d\vec{Q} = -H(t)$$

by the original equation and integration by parts. Now we compute

$$(2.25) \quad \frac{d}{dt} H(t) = \int_{\Omega} e^{-\Psi} \nabla u \nabla u_t d\vec{Q}$$

$$(2.26) \quad = \int_{\Omega} e^{-\Psi} \nabla u \nabla Lu d\vec{Q}$$

$$(2.27) \quad = \int_{\Omega} e^{-\Psi} \nabla u L \nabla u + e^{-\Psi} \nabla u [\nabla L] u d\vec{Q}$$

$$(2.28) \quad = \int_{\Omega} -e^{-\Psi} |\nabla^2 u|^2 + e^{-\Psi} \nabla u (-\nabla^2 \Psi) \nabla u d\vec{Q}$$

$$(2.29) \quad \leq -cH(t).$$

Hence $H(t) \leq H(0)e^{-ct}$. Integrating in time, we get

$$(2.30) \quad D(0) - D(\infty) = \int_0^\infty H(t) dt \leq H(0) \int_0^\infty e^{-ct} dt = \frac{1}{c}H(0).$$

Also, as t approaches infinity, u approaches the stationary constant solution of L . Since $\int e^{-\Psi} u d\vec{Q}$ is a conserved quantity in time, this constant solution will be $\alpha \int e^{-\Psi} f d\vec{Q}$. In addition,

$$(2.31) \quad D(\infty) = \alpha \left(\int e^{-\Psi} f d\vec{Q} \right)^2.$$

We want to point out that although the finite-time existence has been shown in the above without using the above estimate, the latter remains very useful and represents some of the fundamental properties of the Fokker–Planck equations.

REMARK 2. By multiplying (2.7) by $\frac{dg}{dt}$ and performing similar energy estimates, one may extend the regularity of the solution to $L^\infty([0, T]; H_0^1(\Omega) \cap V) \cap H^1([0, T]; L^2(\Omega))$.

REMARK 3. Assuming the existence of classical solutions to (2.5), it is easy to show by a maximum principle argument that the solution remains positive in Ω if the initial condition is such. In fact, if g assumes for the first time a zero local minimum at (\vec{Q}, t) , we then have $g(\vec{Q}, t) = \nabla_{\vec{Q}}g(\vec{Q}, t) = 0$, $\frac{\partial}{\partial t}g(\vec{Q}, t) < 0$, and $\Delta_{\vec{Q}}g(\vec{Q}, t) \geq 0$. But this contradicts (2.5). The uniqueness of the solution to (2.5) is another consequence of the maximum principle. It takes more careful analysis to generalize these arguments to the weak solution of (2.5).

In the estimate of the energy law (2.13), we did not assume any special properties of the velocity gradient κ . In fact, we may improve our results in the special cases when κ is symmetric or antisymmetric. In these cases, the energy can be shown to be dissipative, and thus the energy law enables the existence of a global-in-time solution and the steady-state solution to (2.7). We briefly point out the techniques to exploit the special features of κ . First, if κ is symmetric, $\kappa\vec{Q}$ is then a gradient of the potential $\frac{1}{2}\vec{Q}^T\kappa\vec{Q}$, and thus can be absorbed into the FENE potential by a substitution $\tilde{\Psi} = \Psi - \frac{1}{2}\vec{Q}^T\kappa\vec{Q}$. Replacing Ψ by $\tilde{\Psi}$ in (2.13), the second integral on the right-hand side of (2.13) no longer exists, and the energy is thus dissipative. Furthermore, the steady-state solution can be explicitly written out in this case. Second, if κ is antisymmetric, it is easy to check that the second integral on the right-hand side of (2.13) vanishes again. The following corollary summarizes these findings.

COROLLARY 2.1. *There exists a global solution and a steady-state solution to (2.7) when κ is symmetric or antisymmetric.*

REMARK 4. *Although we have not established the existence of the steady-state solution to the Fokker–Planck equation for a general velocity gradient, our numerical experiences with the Fokker–Planck equation under simple steady shear flow (where κ is neither symmetric nor antisymmetric) seem to suggest that the steady-state solution to the Fokker–Planck equation does exist even for quite large shear rate. The stability analysis we carry out on a simplified FENE-P model later may shed some light on the understanding of the behavior of the stationary solution to the FENE model itself.*

REMARK 5. *We have limited our analysis to the Fokker–Planck equation with a special given velocity gradient. The same technique (of using a transformed variable and using a weighted Sobolev space) can be combined with the methods presented in [18]*

to study the local well-posedness of the fully coupled system as well. Note that similar local existence results were recently presented in Zhang [27] under more restrictive assumptions on b .

REMARK 6. We note that the existence of steady states is also valid for the finite-dimensional Galerkin approximations, and one may also show the convergence of such approximations to the steady-state solutions discussed in Corollary 2.1. Though (2.10) provides a possible numerical scheme for approximating the solution of the Fokker–Planck equation, for instance an approximation based on the spectral methods [22], we discuss an alternative difference method which is simpler while still preserving important properties of the Fokker–Planck equation.

3. Numerical solutions of the FENE model. For general velocity gradient κ , the Fokker–Planck equation cannot be solved analytically. We now describe two alternative strategies to numerically simulate the FENE model: deterministic simulation of the Fokker–Planck equation directly and Monte Carlo simulation of the associated SDE. The algorithms will be used later to compare the polymeric stress prediction of the FENE model and its various closure approximations.

Fokker–Planck simulation. Recently, Lozinski and Chauviere have proposed an efficient spectral method to numerically solve the Fokker–Planck equation with the FENE potential [22, 3]. They solve the Fokker–Planck equation in polar coordinates, and the appropriate boundary conditions are taken into account by a transformation of the unknown similar to (2.4) used in our analysis. They have shown in [3] that for small flow rates, the spectral method is able to capture the solution accurately even with very low spectral resolution. However, getting accurate numerical results would require many more refined meshes when the flow rate increases. For a low level of discretization, numerically oscillatory solutions may arise at large flow rates, and this is also related to the fact that the spectral method does not guarantee the positivity of the PDF. The direct reason for this difficulty with large flow rates is that the exact solution in this case processes huge gradients which are very localized, and a robust scheme for the Fokker–Planck equation with the FENE potential that overcomes this problem is yet to be developed. Leaving this difficulty for future investigation, we present here a simple finite-difference scheme that is appropriate for modest flow rates. The motivation of the scheme is mainly its simplicity and its ability to preserve the unity and positivity of the PDF solution. We have used the scheme in [25] without a very detailed description, which we seek to provide here. The finite-difference scheme presented here is explicit, and it requires further investigation in the future to incorporate implicit time stepping to improve the scheme as far as the stability and positivity preserving are concerned.

We use a regular grid as shown in Figure 3.1. The probability space $\{\vec{Q} : |\vec{Q}| < \sqrt{b}\}$ is discretized on an $M \times M$ regular grid with mesh size $\Delta x = 2\sqrt{b}/M$, where cells outside the admissible space are marked *inactive*. Each active cell is assigned a probability P_{ij}^n defined at the center of the cell, where n denotes the current time step. The discrete probabilities are updated by means of a discrete analogue of the Chapman–Kolmogorov equation

$$(3.1) \quad P_{i,j}^n = (1 - \Gamma_{i,j}^{i-1,j} - \Gamma_{i,j}^{i+1,j} - \Gamma_{i,j}^{i,j-1} - \Gamma_{i,j}^{i,j+1})P_{i,j}^{n-1} \\ + \Gamma_{i,j-1}^{i,j}P_{i,j-1}^{n-1} + \Gamma_{i,j+1}^{i,j}P_{i,j+1}^{n-1} + \Gamma_{i-1,j}^{i,j}P_{i-1,j}^{n-1} + \Gamma_{i+1,j}^{i,j}P_{i+1,j}^{n-1},$$

where $\Gamma_{i,j}^{k,l}$ represents the transition probability from the grid point (i, j) to (k, l) during one time step. Using the Taylor expansion around the cell (i, j) , one may

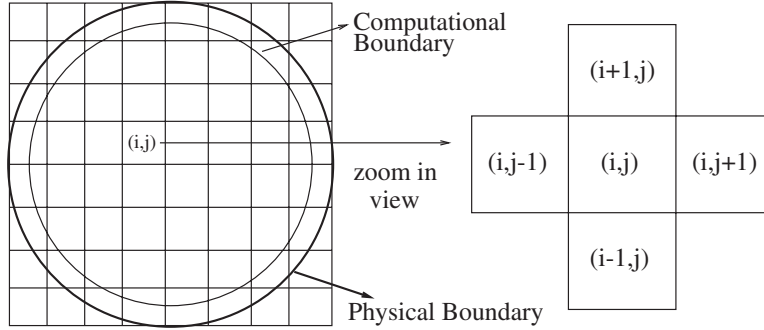


FIG. 3.1. Finite-difference mesh for solving the Fokker–Planck equation. The computational domain is made of the cells contained in the smaller disk.

easily find that the consistency of the finite-difference scheme with the Fokker–Planck equation requires

$$(3.2) \quad \begin{cases} \Gamma_{i,j}^{i,j-1} - \Gamma_{i,j}^{i,j+1} = \left[\frac{1}{2} \left(\frac{Q_1}{1-Q^2/b} \right) - (\kappa_{11}Q_1 + \kappa_{12}Q_2) \right] \frac{\Delta t}{\Delta x}, \\ \Gamma_{i,j}^{i,j-1} + \Gamma_{i,j}^{i,j+1} = \Delta t / \Delta x^2, \\ \Gamma_{i,j}^{i-1,j} - \Gamma_{i,j}^{i+1,j} = \left[\frac{1}{2} \left(\frac{Q_2}{1-Q^2/b} \right) - (\kappa_{21}Q_1 + \kappa_{22}Q_2) \right] \frac{\Delta t}{\Delta x}, \\ \Gamma_{i,j}^{i-1,j} + \Gamma_{i,j}^{i+1,j} = \Delta t / \Delta x^2, \end{cases}$$

where Δt is the time-step size, and the functions on the right-hand side are evaluated at the center of the cell (i, j) . With a no-flux boundary condition (to be discussed later), the scheme automatically conserves the sum of all $P_{i,j}^n$. Furthermore, it preserves the positivity of $P_{i,j}^n$, as long as the transition probabilities $\Gamma_{i,j}^{i,j-1}$, $\Gamma_{i,j}^{i,j+1}$, $\Gamma_{i,j}^{i-1,j}$, and $\Gamma_{i,j}^{i+1,j}$ are all in the range of $[0, 1]$. In view of (3.2), a sufficient condition is

$$(3.3) \quad h \leq \min \left(\left\| \left[\frac{1}{2} \left(\frac{Q_1}{1-Q^2/b} \right) - (\kappa_{11}Q_1 + \kappa_{12}Q_2) \right] \right\|^{-1}, \left\| \left[\frac{1}{2} \left(\frac{Q_2}{1-Q^2/b} \right) - (\kappa_{21}Q_1 + \kappa_{22}Q_2) \right] \right\|^{-1} \right),$$

and $\Delta t \leq h^2$.

Due to the singularity of the FENE force law near the boundary of the configuration space $Q^2 = b$, (3.3) poses an impractical constraint on the mesh size h . To circumvent this problem, we choose to solve the Fokker–Planck equation in a smaller domain with an artificial boundary at $Q^2 = b - \epsilon$, which ensures the existence of a finite Δx verifying (3.3). At the artificial boundary, a no-flux boundary condition is imposed, which can be implemented on the discrete level by setting those transition probabilities to or from grid points violating the constraint $Q^2 < b - \epsilon$ to zero. To analyze the effect of the artificial boundary, we consider a simple case where the velocity gradient κ is symmetric. The steady-state solution to the Fokker–Planck equation (defined on the actual domain $Q^2 < b$) can be explicitly written as $f(Q) = \frac{1}{Z} (1-Q^2/b)^{b/2} \exp(\vec{Q}^T \kappa \vec{Q})$, where $Z = \int_{Q^2 < b} (1-Q^2/b)^{b/2} \exp(\vec{Q}^T \kappa \vec{Q}) d\vec{Q}$ is the normalizing constant. Since this solution satisfies detailed balance [7], the solution to the Fokker–Planck equation on

the artificial domain with a no-flux boundary condition is of the same form, except for a different normalizing constant $Z = \int_{Q^2 < b-\epsilon} (1 - Q^2/b)^{b/2} \exp(\vec{Q}^T \kappa \vec{Q}) d\vec{Q}$. Thus, if the PDF is well concentrated around the origin, as in the case of a moderate velocity gradient, the difference between the solution on the restricted domain and the actual solution is negligibly small. A more rigorous analysis of this effect will be presented elsewhere. We note that, however, for large κ , due to the exponential factor $\exp(\vec{Q}^T \kappa \vec{Q})$, the PDF becomes rather singular and concentrated near the boundary $Q^2 = b$. Though one may choose a smaller ϵ , this would result in extremely small mesh size h because of (3.3). So for large κ , we perform instead Monte Carlo simulation of the SDE associated with the Fokker–Planck equation.

Monte Carlo simulation. To sample the probability space, a sufficiently large number of random walkers are simulated according to the SDE

$$(3.4) \quad d\vec{Q} = \left(\kappa \vec{Q} - \frac{1}{2} \nabla_{\vec{Q}} \Psi \right) dt + d\vec{W}_t.$$

A concern with the brute force way of implementing this SDE (by, for example, the Euler scheme) is that the constraint $|\vec{Q}|^2 < b$ may not be preserved. A nice algorithm that avoids this problem is given by Ottinger [23] in the form of a predictor-corrector scheme. Given \vec{Q}^n at time t_n , the predictor step is to apply the Euler–Maruyama scheme to compute an intermediate value \vec{Q}^* ,

$$(3.5) \quad \vec{Q}^* = \vec{Q}^n + \left(\kappa \vec{Q}^n - \frac{1}{2} \nabla_{\vec{Q}} \Psi(\vec{Q}^n) \right) \Delta t + \Delta \vec{W},$$

where $\Delta \vec{W}$ is a two-dimensional Gaussian random variable whose components have variance Δt . We recall that the force term $\nabla_{\vec{Q}} \Psi = \vec{Q}/(1 - Q^2/b)$. The corrector step that determines \vec{Q}^{n+1} at time $t_{n+1} = t_n + \Delta t$ treats only the force term implicitly and reads

$$(3.6) \quad \left[1 + \frac{\Delta t}{4(1 - (Q^{n+1})^2/b)} \right] \vec{Q}^{n+1} = \vec{Q}^n + \frac{1}{2} \left[\kappa \vec{Q}^* + \kappa \vec{Q}^n - \frac{\vec{Q}^n}{2(1 - (Q^n)^2/b)} \right] \Delta t + \Delta \vec{W}.$$

Notice the same random number is used in (3.5) and (3.6). The length of \vec{Q}^{n+1} can be determined from a cubic equation which, for arbitrary length of the vector on the right-hand side of (3.6), has a unique solution between 0 and \sqrt{b} . Thus, the scheme automatically guarantees the finite-extensibility constraint.

Figure 3.2 gives an example of the steady-state distributions obtained from the Fokker–Planck simulation and the Monte Carlo simulation. The simulation is for shear flow with shear rate equal to 2. The Fokker–Planck equation is solved on a 500×500 grid using the algorithm described above. The Monte Carlo simulation utilizes 10^5 Brownian particles (polymers), and the histogram is constructed on 100×100 bins (regular grid cells in which the numbers of Brownian particles are counted). Note that the purpose of Monte Carlo simulation in practical computation is to produce various ensemble averages rather than the fully detailed probability distribution. In fact, in spite of the noisy appearance of the Monte Carlo histogram, the relative difference between the shear and normal stress predictions obtained by the two approaches is within only 1%. The data to be presented later in this paper are generated by

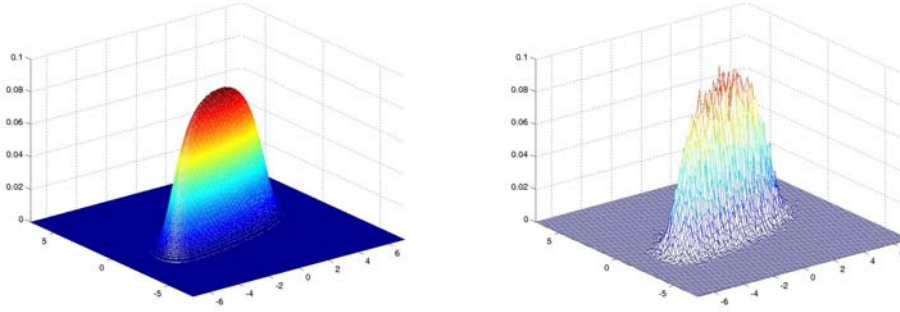


FIG. 3.2. *Steady-state PDFs obtained from simulating the Fokker–Planck equation directly (left) and the Monte Carlo simulation of the associated SDE (right).*

either the Fokker–Planck or Monte Carlo simulation, depending on the magnitude of shear or extension rates.

4. Stability of FENE-P. Both the Fokker–Planck simulation and the Monte Carlo simulation are targeted at resolving or sufficiently sampling the probability space. They are computational very demanding, especially when one is interested in the coupled system of the macroscopic Navier–Stokes equation and the microscopic Fokker–Planck equation. Therefore, model reduction via various moment-closure approximations provides an attractive alternative to the above detailed simulation approaches. In this section, we study the FENE-P closure which is widely adopted in many qualitative numerical studies of the FENE polymeric fluids. The existence of global-in-time solutions to the FENE-P model for a given homogeneous flow has been proven by Jourdain and Lelievre in [12]. In this paper, we focus on the linear stability analysis of the steady-state solution to the FENE-P model. Recall that A denotes the conformation tensor $\langle \bar{Q}\bar{Q}^T \rangle$. In the scaled form, the FENE-P model can be written compactly as

$$(4.1) \quad \frac{\partial A}{\partial t} - \kappa A - A\kappa^T = 1 - \frac{A}{1 - \text{Tr } A/b},$$

where $\text{Tr } A$ is the trace of A . In the one-dimensional case (A is a scalar), it is trivial to see that the ODE has a unique solution in $(0, b)$ which is asymptotically stable.

We now study the two-dimensional case in which the components of A can be rearranged into $M_1 = \langle Q_1^2 + Q_2^2 \rangle$, $M_2 = \langle Q_1^2 - Q_2^2 \rangle$, and $M_3 = \langle Q_1 Q_2 \rangle$. Equation (4.1) becomes

$$(4.2) \quad \begin{cases} \frac{\partial M_1}{\partial t} = (\kappa_{11} - \kappa_{22})M_2 + (\kappa_{12} + \kappa_{21})M_3 + 2 - \frac{M_1}{1 - M_1/b}, \\ \frac{\partial M_2}{\partial t} = (\kappa_{11} - \kappa_{22})M_1 + (\kappa_{12} - \kappa_{21})M_3 - \frac{M_2}{1 - M_1/b}, \\ \frac{\partial M_3}{\partial t} = (\kappa_{12} + \kappa_{21})M_1 - (\kappa_{12} - \kappa_{21})M_2 - \frac{M_3}{1 - M_1/b}. \end{cases}$$

We perform asymptotic analysis on the stability of the system obtained by linearizing (4.2) around its steady-state solution (M_1^*, M_2^*, M_3^*) , which can be solved by setting the time derivatives in (4.2) to zero. The analysis focuses on steady shear flow for the FENE-P model, whereas the theorem presented in the previous section could not guarantee the existence of long-time and steady-state solutions to the FENE model

under steady shear flow. However, the argument can be easily extended to the case of extensional flow.

For simple shear flow $\vec{u} = (\alpha y, 0)$, the velocity gradient simplifies to $\kappa_{12} = \alpha$, and $\kappa_{11} = \kappa_{21} = \kappa_{22} = 0$. The Jacobian of the linearized system evaluated at (M_1^*, M_2^*, M_3^*) is

$$(4.3) \quad \begin{pmatrix} -\frac{1}{(1-M_1^*/b)^2} & 0 & \alpha \\ -\frac{M_2^*/b}{(1-M_1^*/b)^2} & -\frac{1}{1-M_1^*/b} & \alpha \\ \alpha - \frac{M_3^*/b}{(1-M_1^*/b)^2} & -\alpha & -\frac{1}{1-M_1^*/b} \end{pmatrix}.$$

Our goal is to study the asymptotic behavior of the eigenvalues of this matrix as $\alpha \rightarrow \infty$. We need to first describe the asymptotic behavior of M_1^* . It is easy to see that (4.2) implies

$$(4.4) \quad -\frac{M_1^*}{1-M_1^*/b} + 2\alpha^2(1-M_1^*/b)^2 = -2.$$

This equation uniquely determines a solution in $(0, b)$ which, as α increases, approaches b asymptotically. Solving for the leading-order term, we obtain the rate by which M_1^* approaches b in the large shear rate limit:

$$(4.5) \quad 1 - M_1^*/b = (b/2)^{\frac{1}{3}}|\alpha|^{-\frac{2}{3}} + \text{l.o.t.}$$

On the other hand, omitting the lower-order terms, the eigenvalues of (4.3) λ can be shown to satisfy the algebraic equation

$$(4.6) \quad \tilde{\lambda}^3 + \frac{\alpha^{\frac{4}{3}}}{(b/2)^{\frac{2}{3}}}\tilde{\lambda}^2 + \frac{2\alpha^2}{b}\tilde{\lambda} + \frac{\alpha^{\frac{8}{3}}}{(b/2)^{\frac{4}{3}}} = 0,$$

where $\tilde{\lambda} = \lambda + 1/(1 - M_1^*/b)$. We assume that, up to the leading-order terms, (4.6) may be factored as $(\tilde{\lambda} + C_1\alpha^p)(\tilde{\lambda} + C_2\alpha^q)(\tilde{\lambda} + C_3\alpha^r) = 0$, where $p \geq q \geq r$. Comparing with (4.6), we get $p = 4/3$, $q = r = 2/3$, $C_1 = 1/(b/2)^{\frac{2}{3}}$, and $C_2, C_3 = (1 \pm \sqrt{3}i)/2(b/2)^{\frac{1}{3}}$. Thus, all eigenvalues have negative real parts. The “least stable” mode corresponds to the least negative real part of the eigenvalues, and it is

$$(4.7) \quad \text{Re } \lambda \sim -\frac{3}{(b/2)^{\frac{1}{3}}}\alpha^{\frac{2}{3}},$$

which indicates that the steady-state solution of the FENE-P model becomes more stable as the shear rate increases. This is a somewhat surprising result because numerous numerical simulations have indicated that the PDF of the FENE model becomes more singular for larger shear rates. Although it is questionable to relate the present analysis of the FENE-P model to the FENE model, the two models are somehow related in the sense that the preaveraging assumption (1.12) becomes exact if the PDF is a delta distribution in Q , and from numerical studies the PDF of the FENE model seems to approach a delta distribution for large flow rates. Thus assuming that the FENE-P model captures the qualitative behavior of the FENE model at large shear rates, the present analysis suggests that the singular PDFs produced by the FENE model at large shear rates may be rather stable to perturbations.

To validate our calculation, we compare the asymptotic result (4.7) with the numerical evaluation of the eigenvalues of (4.3) using MATLAB. For $b = 50$, the

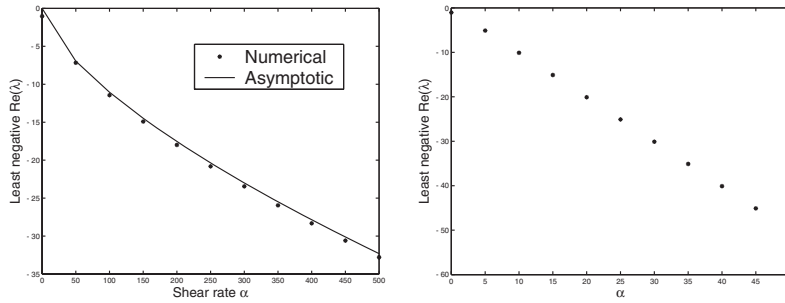


FIG. 4.1. The least negative eigenvalues of the Jacobian matrix (4.3) in shear flow (left) and in a combination of shear and extensional flow (right).

least negative real part of the calculated eigenvalue is plotted against the shear rate α (the left picture of Figure 4.1) as well as the prediction from the asymptotic formula. Excellent agreement is found. Extensional flow can be studied in the same way. In particular, one finds the same pattern that the steady-state solution becomes more stable as the extension rate increases, except that the least negative eigenvalue in this case goes to $-\infty$ linearly. We give another example of a more general flow described by $\kappa_{11} = -\alpha/2$, $\kappa_{12} = \alpha$, $\kappa_{21} = 0$, and $\kappa_{22} = \alpha/2$. The numerical results using MATLAB are shown on the right of Figure 4.1. The pattern that the eigenvalue decays to $-\infty$ as α increases is again observed.

Finally, we mention that the same analysis can be applied to the closure approximation proposed in [25]. The model is motivated by assuming the PDF to be a perturbation from its equilibrium state, and the moment equations are closed based on an ansatz on the perturbed PDF. The model has the advantage of being able to faithfully reproduce the quantitative features of the FENE model for weak flow. In fact, the moment equations are very similar to the FENE-P model:

$$(4.8) \quad \begin{cases} \frac{\partial M_1}{\partial t} = (\kappa_{11} - \kappa_{22})M_2 + (\kappa_{12} + \kappa_{21})M_3 + 2 - \frac{M_1}{1-2M_1/b}, \\ \frac{\partial M_2}{\partial t} = (\kappa_{11} - \kappa_{22})M_1 + (\kappa_{12} - \kappa_{21})M_3 - \frac{1+M_1/b}{1-2M_1/b}M_2, \\ \frac{\partial M_3}{\partial t} = (\kappa_{12} + \kappa_{21})M_1 + (\kappa_{12} - \kappa_{21})M_2 - \frac{1+M_1/b}{1-2M_1/b}M_3. \end{cases}$$

Thus, one may establish the linear stability of the steady-state solutions to this closure approximation using the same method. However, for large velocity gradients, the asymptotic limit of M_1^* of this model is $b/2$, which is an artificial and false constraint on the maximum extensibility of the dumbbell. To combine the quantitative strength of the model proposed in [25] for the flow of small velocity gradients with the more reasonable asymptotic behavior of the FENE-P model, one may, for example, replace $1 - 2M_1/b$ in (4.8) with $1 - \eta(\kappa)M_1/b$, where $\eta(\kappa) \in [1, 2]$ is a phenomenological parameter that can be calibrated against the original FENE model. We leave discussion on such hybrid methods to our future research.

5. A higher-order linear closure model. Most existing closure models involve second-order or, at the most, fourth-order moments. It is a natural question to ask whether including even higher moments can improve the closure approximation to the original FENE model. Based on the framework proposed in [25], we make the following ansatz on the PDF:

$$(5.1) \quad f = \left(1 - \frac{Q^2}{b}\right)^{b/2} \sum_{n=0}^N \sum_{\substack{k+l=2n \\ k \geq 0, l \geq 0}} C^{k,l} Q_1^k Q_2^l.$$

The first factor $(1 - \frac{Q^2}{b})^{b/2}$ is the equilibrium distribution of the FENE model whence the velocity gradient $\kappa = 0$. The second factor is a Taylor polynomial of order $2N$ viewed as a perturbation to the equilibrium distribution due to the nonvanishing velocity gradient in the general case. Note that since the solution to the FENE model is always an even function of \vec{Q} , only even powers of \vec{Q} are included in the Taylor polynomial.

The restricted class of PDFs defined by the ansatz (5.1) is parameterized by $(N + 1)^2$ coefficients $C^{k,l}$, which can be determined, provided that the values of all moments up to order $2N$ are known. More specifically, given the moments $M^{i,j} = \langle Q_1^i Q_2^j \rangle$ for all $i + j = 2n$ and $n = 0, 1, \dots, N$, $C^{k,l}$ may be determined from the following linear system:

$$(5.2) \quad \sum_{n=0}^N \sum_{\substack{k+l=2n \\ k \geq 0, l \geq 0}} C^{k,l} \int \left(1 - \frac{Q^2}{b}\right)^{b/2} Q_1^{k+i} Q_2^{l+j} d\vec{Q} = M^{i,j}, \quad i + j = 2n, n = 0, 1, \dots, N.$$

Owing to the simplicity of (5.1), the integral $\int (1 - \frac{Q^2}{b})^{b/2} Q_1^{k+i} Q_2^{l+j} d\vec{Q} \equiv I^{(i,j),(k,l)}$ can be evaluated analytically. Using polar coordinates, we may rewrite $I^{(i,j),(k,l)}$ as $\int_0^{\sqrt{b}} (1 - \frac{Q^2}{b})^{b/2} Q^{2p+1} dQ \int_0^{2\pi} \cos^{k+i} \theta \sin^{l+j} \theta d\theta$, where $p = (k + l + i + j)/2$. One may easily verify that the radial integral $S(p) = \int_0^{\sqrt{b}} (1 - \frac{Q^2}{b})^{b/2} Q^{2p+1} dQ$ satisfies the recursive formula $S(p) = S(p - 1)bp/(b + b/2 + 1)$, and $S(0) = b/(b + 2)$. A recursive formula for the angular integral can also be easily obtained. To cast (5.2) into matrix form, we denote by I the $(N + 1)^2 \times (N + 1)^2$ stiffness matrix whose $((i, j), (k, l))$ th component is $I^{(i,j),(k,l)}$ (imagine a natural ordering of the double index (i, j) , for example, such that $(i, j) > (k, l)$ if and only if $i + j > k + l$ or $i + j = k + l$ and $i > k$). Obviously, I is symmetric positive-definite. Similarly, let C and M be the $(N + 1)^2$ -dimensional vectors with components $C^{k,l}$ and $M^{k,l}$, respectively. In matrix form, (5.2) reads $IC = M$.

Next, we derive evolution equations for the moments up to order $2N$ based on closure approximations as a consequence of ansatz (5.1). Multiplying the Fokker-Planck equation by $Q_1^i Q_2^j$, where $i + j \leq 2N$, and integrating by parts over the probability space $Q^2 < b$, we have

$$(5.3) \quad \begin{aligned} & \frac{\partial M^{i,j}}{\partial t} - (i\kappa_{11}M^{i,j} + i\kappa_{12}M^{i-1,j+1} + j\kappa_{21}M^{i+1,j-1} + j\kappa_{22}M^{i,j}) \\ & = -\frac{i+j}{2} \int \frac{Q_1^i Q_2^j}{1 - Q^2/b} f(\vec{Q}, t) d\vec{Q} + \frac{i(i-1)}{2} M^{i-2,j} + \frac{j(j-1)}{2} M^{i,j-2}. \end{aligned}$$

The only term requiring closure approximation is the integral $\int \frac{Q_1^i Q_2^j}{1 - Q^2/b} f(\vec{Q}, t) d\vec{Q}$ which, under the assumption that the PDF satisfies the ansatz (5.1), may be represented as

$$(5.4) \quad \int \frac{Q_1^i Q_2^j}{1 - Q^2/b} f(\vec{Q}, t) d\vec{Q} = \sum_{n=0}^N \sum_{\substack{k+l=2n \\ k \geq 0, l \geq 0}} C^{k,l} \int \left(1 - \frac{Q^2}{b}\right)^{b/2-1} Q_1^{k+i} Q_2^{l+j} d\vec{Q}.$$

The integrals on the right-hand side are very similar to those of the stiffness matrix I and can be evaluated analytically. Denoting by J the matrix whose $((i, j), (k, l))$ th component is given by $\frac{i+j}{2} \int (1 - \frac{Q^2}{b})^{b/2-1} Q_1^{k+i} Q_2^{l+j} d\vec{Q}$, we may write (5.3) in its matrix form,

$$(5.5) \quad \frac{\partial M}{\partial t} = -JC + KM = (K - JI^{-1})M,$$

where K is a constant $(N+1)^2 \times (N+1)^2$ matrix defined by $(KM)^{(i,j)} = \frac{i(i-1)}{2} M^{i-2,j} + \frac{j(j-1)}{2} M^{i,j-2} + (i\kappa_{11} M^{i,j} + i\kappa_{12} M^{i-1,j+1} + j\kappa_{21} M^{i+1,j-1} + j\kappa_{22} M^{i,j})$. The polymeric stress $\int \frac{Q \otimes Q}{1-Q^2/b} f(\vec{Q}, t) d\vec{Q}$ can also be represented by the moments in a similar fashion, and it provides a checkpoint to evaluate the current closure approximation in comparison with other closure models. Note that unlike the FENE-P model or the one proposed in [25], the current higher-order closure approximation leads to a *linear* system of evolution equations for the moments M .

It is interesting to remark on the similarity of the present moment-closure strategy and the general spectral Petrov–Galerkin method for numerically solving PDEs. If we make the variable transformation $M = IC$, (5.5) becomes the evolution equation for the parameters $C^{i,j}$ of the ansatz (5.1):

$$(5.6) \quad \frac{\partial C}{\partial t} = I^{-1}(K - JI^{-1})IC.$$

From the derivation of the moment equations, this is exactly the Petrov–Galerkin formulation if the spectral solution space is defined by (5.1) and the test functions are taken to be powers of \vec{Q} up to order $2N$. The advantage of choosing the solution space (5.1) lies in its close relation to the equilibrium distribution, and thus the ability to capture the actual solution to the FENE Fokker–Planck equation for a small velocity gradient. However, the performance of the present closure for larger velocity gradients is not automatically guaranteed by (5.1) and needs to be evaluated using numerical simulation.

To test the proposed closure model, we perform numerical simulations for inception of shear or extension flow with various rates followed by relaxation. The FENE parameter b is chosen to be 50. First, we illustrate for moderate values of shear or extensional rates that increasing the order N of the moments involved does result in better approximation to the FENE model. Taking normal stress as an example, we show the stress growth and relaxation for shear flow with shear rate 2 (left picture in Figure 5.1) and for extension flow with extensional rate 0.7 (right picture in Figure 5.1) for different choices of N , and we compare them with the original FENE model. The same pattern is observed that we get better approximation as the order of moments involved is increased, and perfect agreement with the FENE model is obtained for $N = 3$ in the shear case and $N = 9$ in the extension case. The larger order required in the extension case is due to the stronger tendency for the polymer stretching under an extension flow than that under a shear flow with comparable velocity gradients. We have also verified numerically that the moment-closure model with the above orders gives a perfect agreement for any shear flow with rates less than 2 and any extension flow with rates less than 0.7. We compare the stress predictions with the FENE-P and FENE-L closure models in Figure 5.2. For shear rate 2, both the FENE-L and the FENE-P models overpredict the steady-state value of the normal stress. For extensional rate 0.7, the FENE-L or FENE-P closure produces neither the

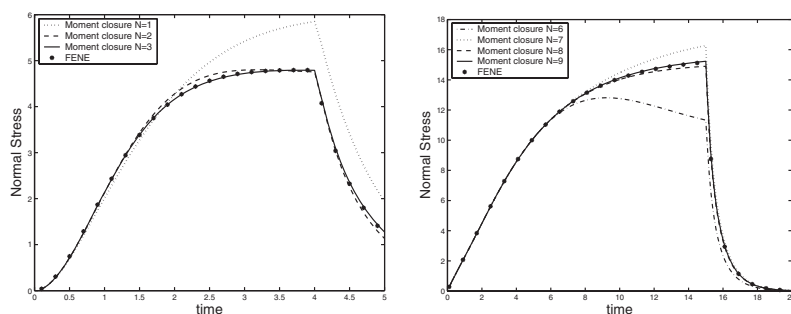


FIG. 5.1. Increasing the order of moments involved does improve the closure approximation. Left: normal stress difference in startup of shear flow with $\kappa_{12} = 2$. Right: normal stress difference in startup of extensional flow with $\kappa_{11} = -\kappa_{22} = 0.7$.

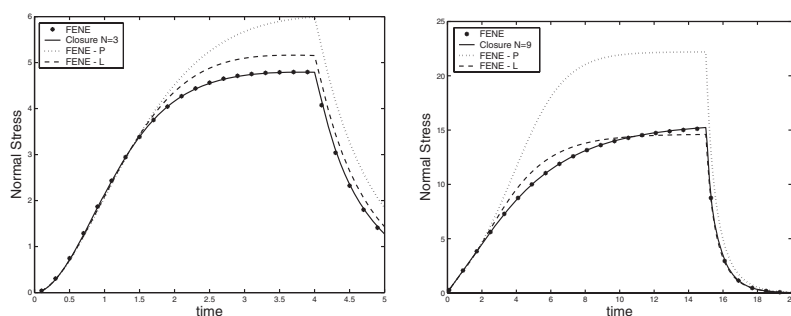


FIG. 5.2. The proposed higher-order closure approximations outperform the FENE-P and FENE-L models for moderate shear or extension rates.

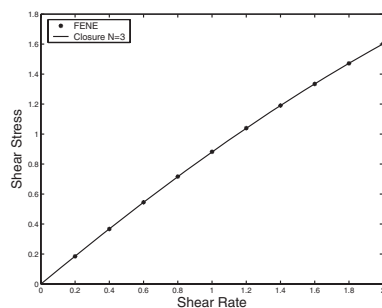


FIG. 5.3. Shear stress prediction by the FENE model and the proposed closure model with $N = 3$.

correct steady-state stress nor the correct time scale to approach the steady state. The proposed higher-order closure approximation clearly outperforms the lower-order methods such as the FENE-P and FENE-L models. At last, we present, for the range of shear rates from 0 to 2, the steady-state shear stress prediction by the proposed closure model with $N = 3$ in Figure 5.3. The point worth noticing is that the slight shear-thinning effect of the FENE model is correctly reproduced by our closure model up to the shear rate 2.

Limitation. The most severe limitation of the proposed linear closure model is that (5.5) becomes unstable for large shear or extensional rates. Taking shear

TABLE 5.1
Largest real part of the eigenvalues of $K - JI^{-1}$.

Shear rate	4	5	6	7	8	9	10
Eigenvalue	-1.7087	0.6670	1.1466	1.5795	1.9858	2.3736	2.7470

flow as an example, for $N = 3$, we may numerically evaluate the eigenvalues of the matrix $(K - JI)^{-1}$ in (5.5) for increasing values of the shear rate. Table 5.1 summarizes the largest real part of the eigenvalues, which changes from being negative (stable) to being positive (unstable) as the shear rate increases. The same pattern is also observed for extension flow and for higher orders of the closure approximation. Since the FENE-P model has been shown to yield stable steady-state solutions and the nonlinear nature of the FENE-P closure approximation has played a crucial role in the analysis, one may speculate that the instability of the proposed method is mainly due to the linear relation between the parameters of the ansatz (5.1) on the PDF and its moments. An alternative explanation lies in the observation that in the original Fokker–Planck equation, the infinitely large eigenvalues of the Laplacian operator provide a control mechanism over arbitrarily large velocity gradients. In contrast, in a linear closure approximation where only a finite number of moments are taken, the sequence of eigenvalues of the Laplacian operator is cut finite, and thus can no longer act as a stabilizing factor against the increasing κ . There is yet another intuitive interpretation of the deficiency of the proposed closure model for large velocity gradients. As shown in Figure 5.4, the steady-state probability distribution to the FENE model (via Monte Carlo simulation) under strong extension flow $\kappa_{11} = -\kappa_{22} = 1$ displays a rather singular shape. The insufficiency of the ansatz (5.1) to incorporate such singular shapes may be a direct reason for the failure of the proposed method for large velocity gradients.

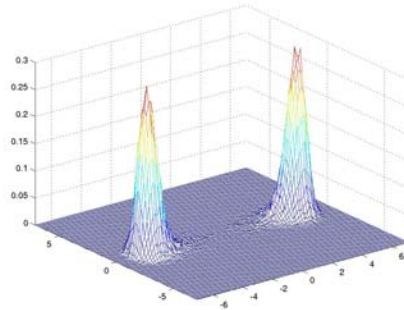


FIG. 5.4. The steady-state PDF from Monte Carlo simulation of the FENE model under extension flow $\kappa_{11} = -\kappa_{22} = 1$.

Generally speaking, one would not expect a closure approximation to reproduce the original model at all regimes of the physical parameters. Depending on practical interests, a satisfactory closure model is to yield quantitative agreement with the original model at a certain regime of parameters and still retain its stability for other regimes. It is left for our future work to investigate how to improve the stability of the present linear closure model by introducing suitable nonlinearity or singular shapes to the ansatz (5.1).

6. Conclusion. In this paper, we have addressed several analytical and numerical issues of the FENE model of polymeric fluids. On the analytical side, we have established the finite-time well-posedness of the Fokker–Planck equation for general velocity gradients κ . Although we have only been able to establish long-time asymptotic results for special symmetric or antisymmetric κ , we speculate that this is still true for general κ . The speculation is partly based on stability analysis of the FENE-P closure model, for which we have shown that the steady-state solution becomes even more stable as the shear or extension rate increases. On the numerical side, we have presented a linear closure model allowing for systematic inclusion of higher-order moments. The model has its advantage of being able to more faithfully reproduce the quantitative behavior of FENE for moderate shear and extension rates. But the model is shown to become unstable for large shear or extension rates. The question of how to improve the stability of the model by introducing appropriate nonlinear effects or singular PDF shapes will be a major focus of our future research.

REFERENCES

- [1] J. W. BARRETT, C. SCHWAB, AND E. SULI, *Existence of global weak solutions for some polymeric flow models*, M3AS: Mathematical Models and Methods in Applied Sciences, 15 (2005), pp. 939–983.
- [2] R. B. BIRD, O. HASSAGER, R. C. ARMSTRONG, AND C. F. CURTISS, *Dynamics of Polymeric Fluids, Vol. 2, Kinetic Theory*, John Wiley and Sons, New York, 1977.
- [3] C. CHAUVIERE AND A. LOZINSKI, *Simulation of dilute polymer solutions using a Fokker-Planck equation*, Comput. & Fluids, 33 (2004), pp. 687–696.
- [4] P. DEGOND, M. LEMOU, AND M. PICASSO, *Viscoelastic fluid models derived from kinetic equations for polymers*, SIAM J. Appl. Math., 62 (2002), pp. 1501–1519.
- [5] M. DOI AND S. F. EDWARDS, *The Theory of Polymer Dynamics*, Clarendon Press, Oxford, UK, 1986.
- [6] W. E, T. LI, AND P. ZHANG, *Well-posedness for the dumbbell model of polymeric fluids*, Comm. Math. Phys., 248 (2004), pp. 409–427.
- [7] C. W. GARDINER, *Handbook of Stochastic Methods*, 2nd ed., Springer-Verlag, Berlin, 1997.
- [8] M. GURTIN, *An Introduction to Continuum Mechanics*, Academic Press, New York, 1981.
- [9] P. HALIN, G. LIELENS, R. KEUNINGS, AND V. LEGAT, *The Lagrangian particle method for macroscopic and micro-macro viscoelastic flow computations*, J. Non-Newtonian Fluid Mech., 79 (1998), pp. 387–403.
- [10] M. HULSEN, A. VAN HEEL, AND B. VAN DEN BRULE, *Simulation of viscoelastic flows using Brownian configuration fields*, J. Non-Newtonian Fluid Mech., 70 (1997), pp. 79–101.
- [11] B. JOURDAIN AND T. LELIEVRE, *Mathematical analysis of a stochastic differential equation arising in the micro-macro modeling of polymeric fluids*, in Probabilistic Methods in Fluids, I. M. Davies, N. Jacob, A. Truman, O. Hassan, K. Morgan, and N. P. Weatherill, eds., World Scientific, River Edge, NJ, 2003, pp. 205–223.
- [12] B. JOURDAIN AND T. LELIEVRE, *Convergence of a Stochastic Particle Approximation of the Stress Tensor for the FENE-P Model*, preprint.
- [13] B. JOURDAIN, C. LE BRIS, AND T. LELIEVRE, *On a variance reduction technique for the micro-macro simulations of polymeric fluids*, J. Non-Newtonian Fluid Mech., 122 (2004), pp. 91–106.
- [14] B. JOURDAIN, T. LELIEVRE, AND C. LE BRIS, *Existence of solution for a micro-macro model of polymeric fluid: The FENE model*, J. Funct. Anal., 209 (2004), pp. 162–193.
- [15] M. LASO AND H. C. OTTINGER, *Calculation of viscoelastic flow using molecular models: The CONNFESSIT approach*, J. Non-Newtonian Fluid Mech., 47 (1993), pp. 1–20.
- [16] G. LIELENS, P. HALIN, I. JAUMAIN, R. KEUNINGS, AND V. LEGAT, *New closure approximations for the kinetic theory of finitely extensible dumbbells*, J. Non-Newtonian Fluid Mech., 76 (1998), pp. 249–279.
- [17] G. LIELENS, R. KEUNINGS, AND V. LEGAT, *The FENE-L and FENE-LS closure approximations to the kinetic theory of finitely extensible dumbbells*, J. Non-Newtonian Fluid Mech., 87 (1999), pp. 179–196.
- [18] F. LIN, C. LIU, AND P. ZHANG, *On hydrodynamics of viscoelastic fluids*, Comm. Pure Appl. Math., to appear.

- [19] F. LIN, C. LIU, AND P. ZHANG, *On Multi-scale Dumbbell Models in Polymer Fluids*, preprint.
- [20] T. LI, H. ZHANG, AND P. ZHANG, *Local existence for the dumbbell model of polymeric fluids*, *Comm. Partial Differential Equations*, 29 (2004), pp. 903–923.
- [21] C. LIU AND N. J. WALKINGTON, *An Eulerian description of fluids containing visco-hyperelastic particles*, *Arch. Ration. Mech. Anal.*, 159 (2001), pp. 229–252.
- [22] A. LOZINSKI AND C. CHAUVIERE, *A fast solver for Fokker-Planck equation applied to viscoelastic flows calculations: 2d FENE model*, *J. Comput. Phys.*, 189 (2003), pp. 607–625.
- [23] H. C. OTTINGER, *Stochastic Processes in Polymeric Fluids, Tools and Examples for Developing Simulation Algorithms*, Springer-Verlag, Berlin, 1996.
- [24] R. TEMAM, *Navier-Stokes Equations*, North-Holland, Amsterdam, 1984.
- [25] P. YU, Q. DU, AND C. LIU, *From micro to macro dynamics via a new closure approximation to the FENE model of polymeric fluids*, *Multiscale Model. Simul.*, 3 (2005), pp. 895–917.
- [26] P. YUE, J. FENG, C. LIU, AND J. SHEN, *A diffuse-interface method for simulating two-phase flows of complex fluids*, *J. Fluid Mech.*, 515 (2004), pp. 293–317.
- [27] P. ZHANG, *private communication*, 2004.
- [28] Q. ZHOU AND R. AKHAVAN, *A comparison of FENE and FENE-P dumbbell and chain models in turbulent flow*, *J. Non-Newtonian Fluid Mech.*, 109 (2003), pp. 115–155.